Localized Heating of the Martian Topside Ionosphere Through the Combined Effects of Magnetic Pumping by Large-Scale Magnetosonic Waves and Pitch Angle Diffusion by Whistler Waves

C. M. Fowler, O. V. Agapitov, S. Xu, D. L. Mitchell, L. Andersson, A. Artemyev, J. Espley, R. E. Ergun, C. Mazelle

▶ **To cite this version:**

C. M. Fowler, O. V. Agapitov, S. Xu, D. L. Mitchell, L. Andersson, et al.. Localized Heating of the Martian Topside Ionosphere Through the Combined Effects of Magnetic Pumping by Large-Scale Magnetosonic Waves and Pitch Angle Diffusion by Whistler Waves. Geophysical Research Letters, 2020, 47, 10.1029/2019GL086408 . insu-03673166

HAL Id: insu-03673166
https://insu.hal.science/insu-03673166

Submitted on 20 May 2022

HAL is a multi-disciplinary open access archive for the deposit and dissemination of scientific research documents, whether they are published or not. The documents may come from teaching and research institutions in France or abroad, or from public or private research centers.

L'archive ouverte pluridisciplinaire **HAL**, est destinée au dépôt et à la diffusion de documents scientifiques de niveau recherche, publiés ou non, émanant des établissements d'enseignement et de recherche français ou étrangers, des laboratoires publics ou privés.

Copyright

Check for updates

AGU100 ADVANCING EARTH AND SPACE SCIENCE

Geophysical Research Letters

RESEARCH LETTER
10.1029/2019GL086408

Key Points:
- Large-scale magnetosonic waves heat ionospheric electrons via the generation of whistler waves and subsequent wave-particle interactions
- The observed heating mechanism demonstrates energy transfer from the solar wind to the Mars upper ionosphere
- Such a heating mechanism may be important at other unmagnetized bodies such as Venus and comets

Supporting Information:
- Supporting Information S1

Correspondence to:
C. M. Fowler,
cmfowler@berkeley.edu

Citation:
Fowler, C. M., Agapitov, O. V., Xu, S., Mitchell, D. L., Andersson, L., Artemyev, A.V, et al. (2020). Localized heating of the Martian topside ionosphere through the combined effects of magnetic pumping by large-scale magnetosonic waves and pitch angle diffusion by whistler waves. *Geophysical Research Letters*, *47*, e2019GL086408. https://doi.org/10.1029/2019GL086408

Received 25 NOV 2019
Accepted 19 FEB 2020
Accepted article online 20 FEB 2020

©2020. American Geophysical Union. All Rights Reserved.

Localized Heating of the Martian Topside Ionosphere Through the Combined Effects of Magnetic Pumping by Large-Scale Magnetosonic Waves and Pitch Angle Diffusion by Whistler Waves

C. M. Fowler[1], O. V. Agapitov[1], S. Xu[1], D. L. Mitchell[1], L. Andersson[2], A. Artemyev[3], J. Espley[4], R. E. Ergun[2], and C. Mazelle[5]

[1]Space Sciences Laboratory, University of California, Berkeley, Berkeley, CA, USA, [2]Laboratory of Atmospheric and Space Physics, University of Colorado Boulder, Boulder, CO, USA, [3]Institute of Geophysics and Planetary Physics, University of California, Los Angeles, Los Angeles, CA, USA, [4]NASA Goddard Space Flight Center, Greenbelt, MD, USA, [5]IRAP, University of Toulouse-CNRS-UPS-CNES, Toulouse, France

Abstract We present Mars Atmosphere and Volatile EvolutioN (MAVEN) observations of periodic (~25 s) large-scale (hundreds of km) magnetosonic waves propagating into the Martian dayside upper ionosphere. These waves adiabatically modulate the superthermal electron distribution function, and the induced electron temperature anisotropies drive the generation of observed electromagnetic whistler waves. The localized (in altitude) minimum in the ratio f_{pe}/f_{ce} provides conditions favorable for the local enhancement of efficient wave-particle interactions, so that the induced whistlers act back on the superthermal electron population to isotropize the plasma through pitch angle scattering. These wave-particle interactions break the adiabaticity of the large-scale magnetosonic wave compressions, leading to local heating of the superthermal electrons during compressive wave "troughs." Further evidence of this heating is observed as the subsequent phase shift between the observed perpendicular-to-parallel superthermal electron temperatures and compressive wave fronts. This heating mechanism may be important at other unmagnetized bodies.

1. Introduction

Wave-particle interactions can be important sources of heating for space plasmas. Cyclotron resonance and Landau damping, for example, can efficiently heat plasmas in a variety of environments, including tokamak experiments (Adam, 1987; Porkolab et al., 1984; Seo et al., 2000), the terrestrial ionosphere and magnetosphere (André & Yau, 1997; Agapitov et al., 2015, 2016), and other planetary magnetospheres and ionospheres such as at Venus (Taylor et al., 1979) and Mars (Ergun et al., 2006; Lundin et al., 2006). Magnetic pumping can also heat plasmas via adiabatically heated anisotropic electron distributions, which relax to Maxwellians through Coulomb collisions and/or efficient pitch angle diffusion (Borovsky & Hansen, 1990; Laroussi & Roth, 1989; Lichko et al., 2017).

For the specific case of magnetic pumping, the Coulomb collision rate in planetary magnetospheres, the solar wind, and upper planetary ionospheres can be small compared to the time period of the forcing magnetic compressions. Other pitch angle diffusion mechanisms, such as wave-particle interactions, are then necessary to achieve the break in adiabaticity of the plasma so that heating can occur. A sufficient level of pitch angle diffusion in such systems can be provided by fast plasma diffusion containing localized heating (Lichko et al., 2017); by radial diffusion on magnetohydrodynamic (MHD) waves, as in the Earth's magnetosphere (Brautigam & Albert, 2000; Barker et al., 2005; Miyoshi et al., 2003, 2006); or by pitch angle diffusion from wave-particle interactions (Artemyev et al., 2016; Agapitov et al., 2019; Borovsky et al., 2017). This study focuses on wave-particle interactions provided by whistler waves, which are known to be capable of producing effective pitch angle diffusion over a wide energy range (Agapitov et al., 2019; Artemyev et al., 2016; Horne et al., 2005; Li et al., 2014; Lyons et al., 1972; Summers et al., 1998). Additionally, whistler waves themselves can be generated as a result of anisotropic plasma compression from magnetic pumping (Agapitov et al., 2018; Drake et al., 2015).

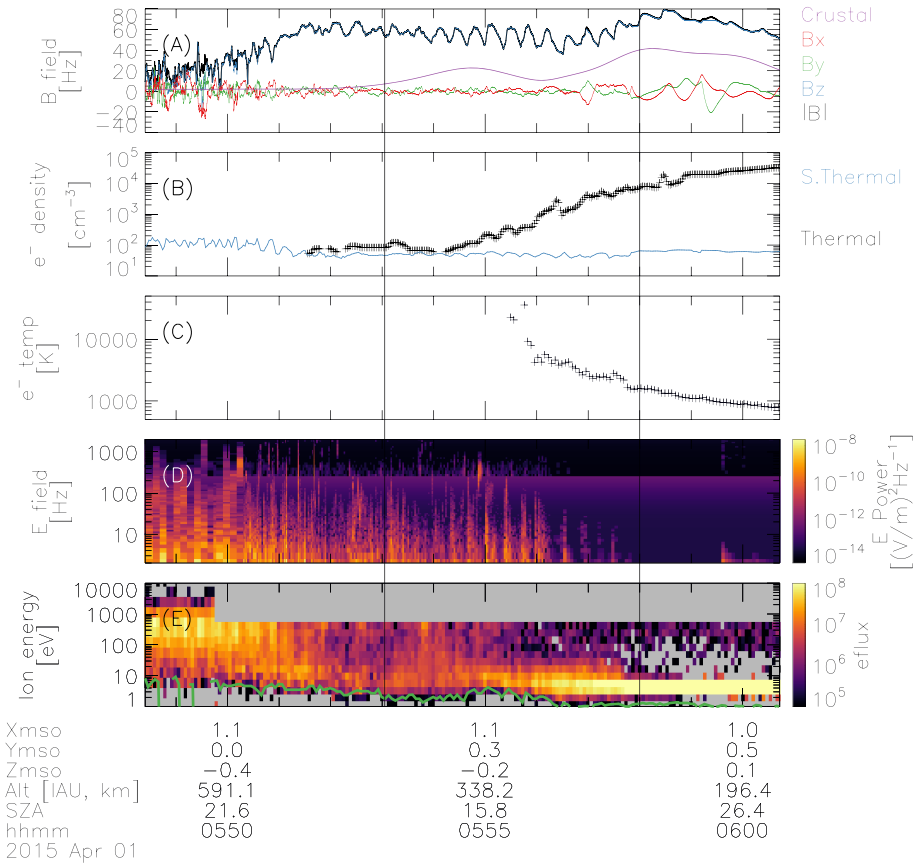

Figure 1. Overview of MAVEN plasma data. (a) Magnetic field information: black = field magnitude; blue = field component parallel to background field; green and red = field components perpendicular to background field; purple = crustal magnetic field model from Morschhauser et al. (2014). (b) Thermal electron density (black) and superthermal electron density (blue). (c) Thermal electron temperature. (d) Combined active and passive electric field wave spectra: spectrogram "slices" alternate in time between the two modes. (e) Omnidirectional ion energy spectrum for all ion species. The spacecraft potential (green line) and spacecraft velocity are not corrected for. E flux has units of eV $(eV \cdot cm^2 \cdot s \cdot sr)^{-1}$.

We present here Mars Atmosphere and Volatile EvolutioN (MAVEN) observations demonstrating that an externally driven fast MHD wave modulates plasma conditions in the Martian upper ionosphere. The resulting anisotropic superthermal electrons generate (observed) whistler waves, which we show produce efficient pitch angle diffusion of the superthermal electron population via wave-particle interactions. This pitch angle diffusion breaks the adiabaticity of the large-scale magnetic compressions, leading to heating of the superthermal electron population.

The data products analyzed in this study are described in section 2. An overview of the MAVEN periapsis pass studied is given in section 3, while a detailed analysis of the wave environment and subsequent localized electron heating is presented in section 4. We discuss our results in the broader context of the Martian ionospheric energy budget in section 5, before concluding in section 6.

2. Description of Data Analyzed

Data analyzed in this study are from the MAVEN mission, which began science operations at Mars in October 2014. MAVEN is a dedicated aeronomy mission in a ~4.5 hr elliptical orbit that precesses over time to provide full local time, latitude, and longitude coverage of the planet (Jakosky et al., 2015). Its orbit has a periapsis altitude of ~150 km and apoapsis altitude close to 6,400 km, meaning that MAVEN at times samples the upstream solar wind, magnetosheath, and dayside ionosphere on a single periapsis pass. The magnetometer (MAG) measures the 3-D vector magnetic field at 32 Hz with a measurement uncertainty of ~0.01 nT (Connerney et al., 2015). Superthermal electrons are measured by the Solar Wind Electron Analyzer

(SWEA) instrument, which is a top hat electrostatic analyzer utilizing electrostatic deflectors to provide a field of view of 360° × 120° (Mitchell et al., 2016). SWEA measures electrons between energies of 3 eV and 5 keV with ($\Delta E/E$) equal to 17%. On ground processing using software provided by the SWEA instrument team enables pitch angle distribution, density, and temperature products to be derived. The Langmuir Probe and Waves (LPW) instrument measures the cold thermal electron population in the ionosphere via two separate Langmuir Probes, mounted on ~7 m booms separated by an angular distance of 110° (Andersson et al., 2015). Thermal electron densities and temperatures derived using the fitting process outlined in Ergun et al. (2015) are analyzed in this study. Active and passive wave spectra obtained in waves mode are also analyzed (Fowler et al., 2017). The SupraThermal And Thermal Ion Composition (STATIC) instrument measures ions between energies below 1 eV up to 30 keV (McFadden et al., 2015). STATIC is an electrostatic top hat analyzer combined with time of flight capabilities that allow it to distinguish ion mass; electrostatic deflectors provide a field of view of 360° × 90°.

3. Overview of Heating Event

Overview time series plasma data of the event analyzed in this study are shown in Figure 1. Data are from an inbound segment of MAVENs orbit, where the spacecraft is close to the subsolar point on the dayside of the planet. Data from this inbound orbit segment were analyzed by Fowler et al. (2018), who demonstrated that compressive, large-amplitude magnetosonic waves, likely generated by the Mars-solar wind interaction, propagate planetward and heat the dayside ionospheric ions. Bursts of whistler waves were observed coincident with the large-amplitude magnetosonic compressive wave fronts in the upper ionosphere (Figure 1, ~05:55–05:58 in particular), but these whistler bursts were not studied in detail and are the focus of this present study.

MAVEN is in the magnetosheath region at around 05:50 UTC, where shocked ions and superthermal electrons are observed. The spacecraft transitions into the ionosphere at around 05:52, when the thermal electron density is first observed by LPW. This density gradually increases until MAVEN samples the cold, dense ionosphere at around 05:58, as demonstrated by the beam of cold (<10 eV) ions observed by STATIC. The compressive, magnetosonic waves discussed by Fowler et al. (2018) are observed between about 05:52 and 05:59 in the magnetic field data. The focus of this study are the bursts of wave power observed in panel (d) between the two black vertical lines, and their effects on the surrounding localized plasma.

4. Detailed Analysis of the Local Plasma Conditions

4.1. Evidence of Magnetic Pumping and Plasma Heating

Time series plasma data measured between the two vertical black lines in Figure 1 are shown in Figure 2. The magnitude of the magnetic field is shown in panel (a). Superthermal electron information is shown in panels (b) to (e): the omnidirectional energy spectrum (b); derived temperatures perpendicular (red) and parallel (black) to the local magnetic field (c); the ratio of these temperatures (d); and the pitch angle distributions (PADs) for energies between 50 and 70 eV (e). LPW wave spectra are shown in panel (f) and an estimate of the whistler wave electric field amplitude based on this is shown in panel (g). The wave amplitude is calculated over the frequency range 0.25 f_{ce} to f_{ce}, where f_{ce} is the electron cyclotron frequency, equal to about 1,500 Hz (Figure 2f). The whistler bursts are observed above frequencies of ~100 Hz (~0.1 f_{ce}), which lie outside the sampling range of the MAG instrument. Consequently, estimates of the whistler magnetic field wave amplitudes (panel g) and whistler wave energy density (panel h) are based on results from Artemyev et al. (2015), when the noise level is small. We provide an overview of this technique in the supporting information. It is unclear which wave modes exist below ~50 Hz in Figure 2f, as these lie below the lower hybrid frequency and by definition are not whistlers. We have not investigated these waves further here.

The observed externally driven fast MHD wave (Figure 2a) has an amplitude of about 10 nT (~20% of the background magnetic field magnitude, $B_0 = 50$ nT), and a frequency of ~0.04 Hz. Such a wave is analogous to compressional magnetic pumping of the plasma. Significant quasiperiodic modulation of the superthermal electron pitch angle distribution function (panel e) occurs as a result of these magnetic compressions and the conservation of the first magnetic adiabatic invariant. Corresponding modulation of the superthermal electron temperatures perpendicular and parallel to the magnetic field are shown in panels (c) and (d). The "cleanest" pitch angle modulation was observed in the 50–70 eV energy range (due to large counting

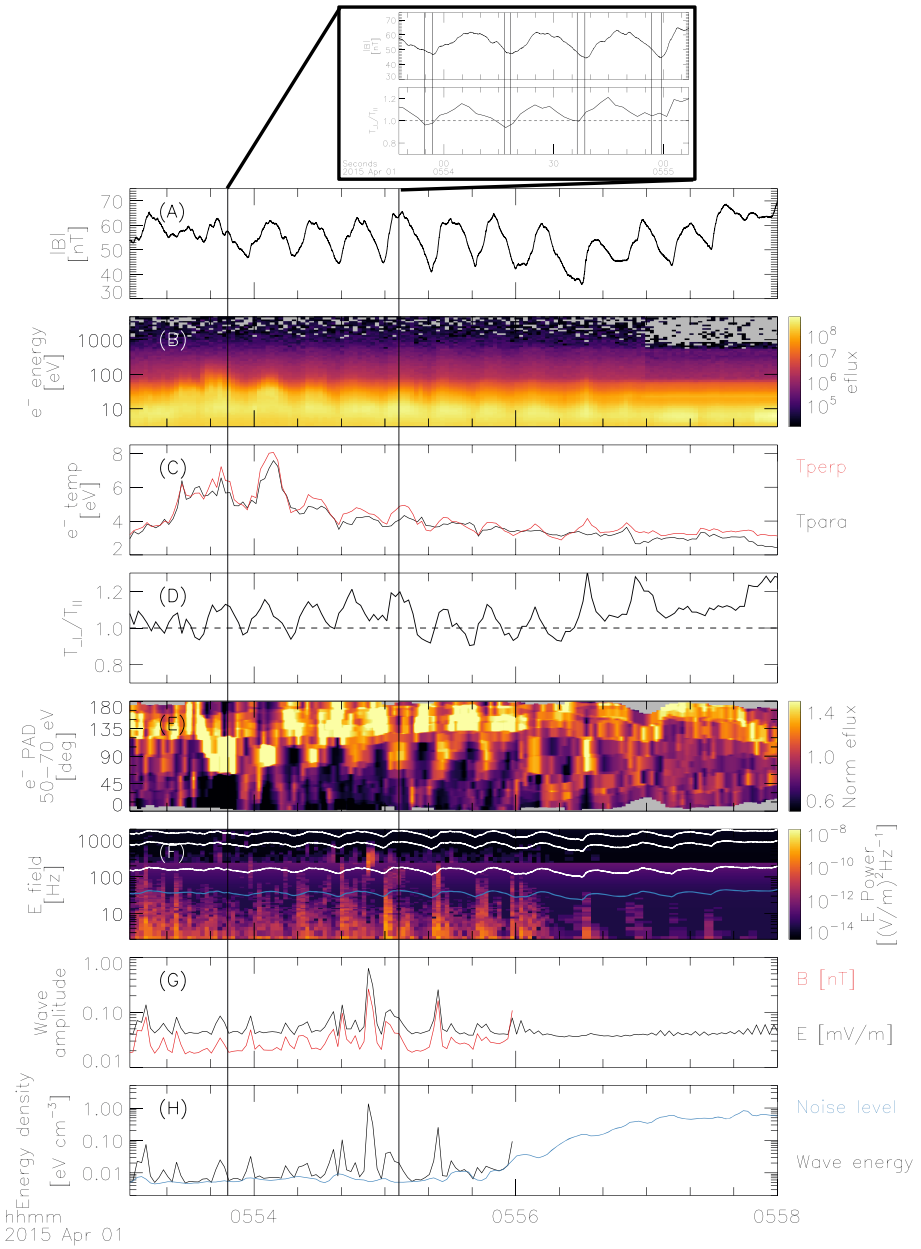

Figure 2. MAVEN time series plasma data from between the two vertical black lines in Figure 1. See section 4 for detailed panel descriptions. The frequencies f_{ce}, 0.5 f_{ce} and 0.1 f_{ce} are overplotted as the white lines in panel (f), while the blue line is the lower hybrid frequency. The insert shows the observed phase difference between the magnetosonic wave and superthermal electron temperature anisotropies.

statistics at these energies), but similar behavior was observed for all superthermal electron energies below ~300 eV (not shown here).

The temperature anisotropy observed in Figure 2d triggers the generation of electromagnetic whistler waves, observed in the frequency range 0.1–0.5 f_{ce} (Figure 2f). Perturbations are also observed in the magnetic field power spectrum, but are not shown here as the MAG power spectrum only samples up to 16 Hz. Following Kennel and Petschek (1966), in a cold plasma the dispersion relation of whistler waves can be written in the following form:

$$\frac{c^2k^2}{\omega^2} = 1 - \frac{\omega_{pi}^2}{\omega(\omega + \Omega_{ci})} - \frac{\omega_{pe}^2}{\omega(\omega + \Omega_{ce})}$$

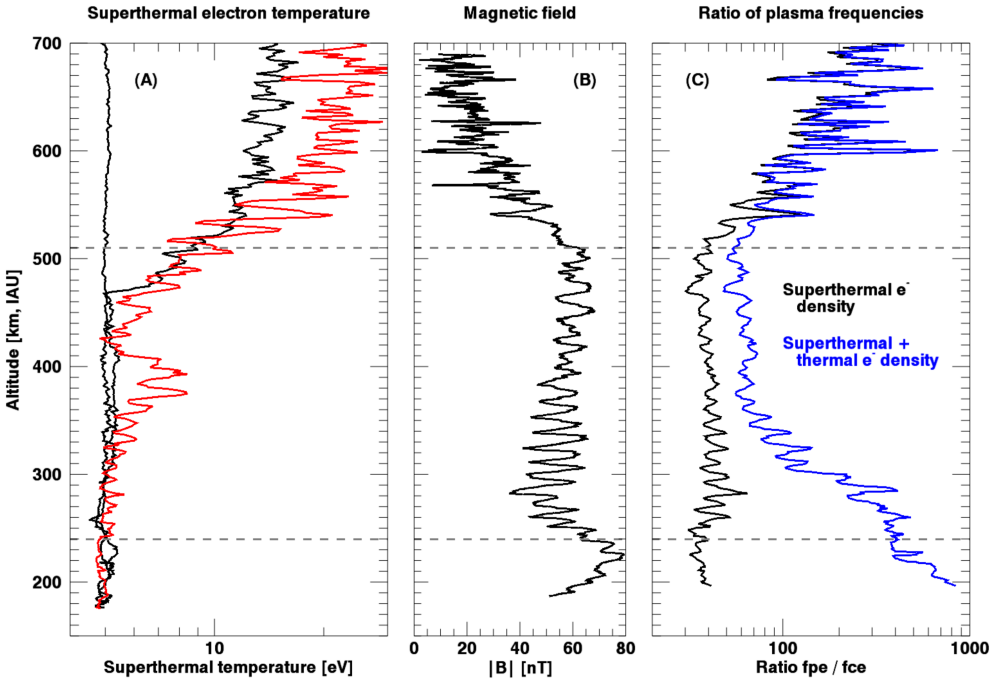

Figure 3. Altitude profiles for various quantities during the studied event. (a) Superthermal electron temperatures for this pass (red) and two neighboring passes in time when magnetosonic waves were not observed (black). (b) Magnitude of magnetic field. (c) Ratio of f_{pe}/f_{ce}, using superthermal electron density (black) and superthermal plus thermal electron density (blue). The dashed horizontal lines mark the approximate region where whistler waves are observed in Figure 2.

where ω is the wave frequency; k is the wave vector; and $\Omega_{ce,i}$ is the local cyclotron frequency of electrons and ions ($\Omega_{ce,i} = \mp\frac{eB}{m_{e,i}}$). When $\Omega_{ci} \ll \omega < |\Omega_{ce}|$, the ion term in the dispersion relation is a factor m_e/m_i smaller than the electron contribution and may be neglected. Additionally, if $|\Omega_{ce}| \ll \omega_{pe}$, (the phase velocity is much less than the velocity of light), then the approximation $c^2k^2/\omega^2 = \omega_{pe}^2/(\omega(\omega+\Omega_{ce}))$ can be used. For the case of a velocity distribution that can be represented as a product of Gaussians with different temperatures for perpendicular and parallel velocities, and a transverse anisotropy exits ($T_{perp} > T_{para}$), the system can be unstable to whistler generation through the cyclotron instability if $T_{perp}/T_{para} - 1 > \omega/(\Omega_{ce} - \omega)$ (Kennel & Petschek, 1966). These conditions are observed during compression periods in this study (Figure 2d) and lead to the observed local generation of whistlers (the expression for the growth rate is presented in the supporting information).

When efficient wave-particle interactions are present, whistler waves act to isotropize electrons (reducing T_{perp} toward T_{para}) via pitch angle diffusion (Kennel & Petschek, 1966). If this isotropization occurs during the magnetic compression fronts observed in Figure 2a, the adiabaticity of the large-scale magnetic pumping is broken, and the superthermal electrons will gain energy during magnetic decompression (i.e., a wave "trough") (Borovsky et al., 2017; Lichko et al., 2017). This heating causes a phase shift between the ratio of perpendicular-to-parallel electron temperatures, and the compressional wave fronts, and such a phase shift of approximately $\frac{\pi}{5}$ is observed in the inset in Figure 2. This phase shift suggests that the magnetic pumping and heating mechanism is present (Lichko et al., 2017), and we provide additional evidence for this interpretation in the following sections and the supporting information.

4.2. Evidence of Efficient Pitch Angle Diffusion via Whistler Waves

Altitude profiles of several additional quantities are shown in Figure 3. Omnidirectional superthermal electron temperatures from several MAVEN periapsis passes are shown in panel (a). There is a clear enhancement in the superthermal electron temperature for this event (red) when the magnetic compressions (shown in panel b) are present, particularly at altitudes between ~350 and 400 km. The ratio of the electron plasma frequency (f_{pe}) divided by the electron cyclotron frequency (f_{ce}) is shown in Figure 3c. The quantity f_{pe}/f_{ce} is important as it determines the efficiency of wave-particle interactions (Summers et al., 1998), whistler wave growth rate (Gary & Wang, 1996), and pitch angle and energy diffusion rates

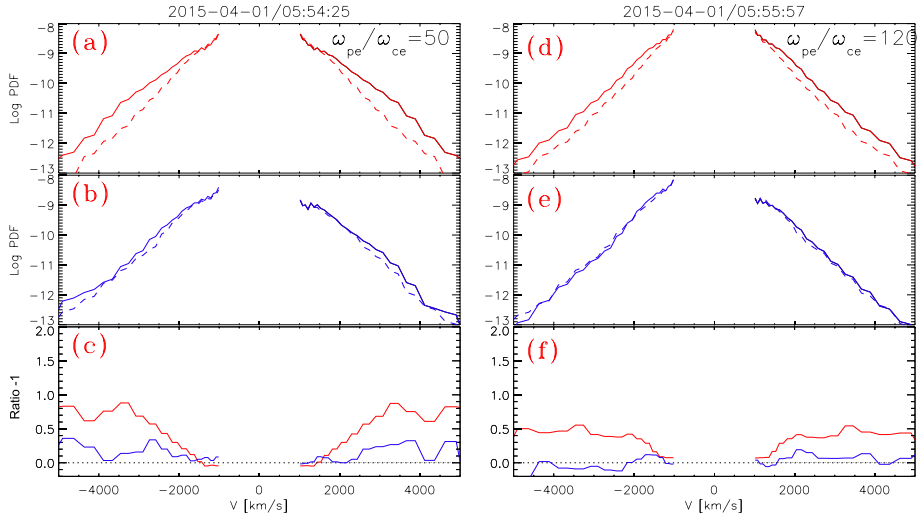

Figure 4. Electron distribution function transverse (red lines) and parallel (blue lines) to the background local magnetic field direction, at times corresponding to maxima (solid lines) and minima (dashed lines) in the magnetic field magnitude. Panels (c) and (f) present the ratio of maximum to minimum (solid divided by dashed) distribution function values for the transverse (red) and parallel (blue) cases, minus 1. The left column presents the data when f_{pe}/f_{ce}~50; the right column when f_{pe}/f_{ce}~120.

(Agapitov et al., 2019; Horne et al., 2003; Summers et al., 1998). Quantities are defined as $f_{pe} = \frac{1}{2\pi}\sqrt{\frac{n_e e^2}{m_e \epsilon_0}}$ and $f_{ce} = \frac{eB}{2\pi m_e}$, where n_e is the electron density, m_e is the electron mass, e is the fundamental charge, B is the magnetic field amplitude and ϵ_0 is the permittivity of free space.

The wave normal angle of the observed whistlers is unknown, and subsequently pitch angle diffusion rates were estimated over a reasonable range of frequencies (up to 0.6 f_{ce}) and wave normal angles, making use of the estimation technique presented in Artemyev et al. (2013). The pitch angle diffusion rate for f_{pe}/f_{ce}~50 is about an order of magnitude larger than that for ratio values of ~120, and the wave normal angle cannot exceed 65–70° for the observed local plasma conditions (because the wave group velocity goes to zero above these values). Such results suggest that these whistler waves can be generated with high wave normal angles relative to the background magnetic field direction and can provide efficient pitch angle diffusion for the event studied here (Agapitov et al., 2015; Artemyev et al., 2016; Mourenas et al., 2015).

The estimated whistler wave energy density (Figure 2h) can be as large as an eV cm^{-3} during whistler wave amplitude peaks, and the corresponding estimated pitch angle diffusion rates for pitch angles between ~70–90° (i.e., electrons that have been abiabatically scattered by the compressive wave) are $D_{\alpha\alpha} = (1\text{–}5) \times 10^{-3}$ s^{-1} and decrease by at least an order of magnitude as the ratio f_{pe}/f_{ce} increases to 200 (see details provided in the supporting information). Lichko et al. (2017) reported that the ratio $\frac{D_{\alpha\alpha}}{f_{MHD}}$ (where f_{MHD} is the MHD fast mode wave frequency, ~0.04 Hz for this study) peaks just below 0.2 for maximum electron heating efficiency. For this event, $\frac{D_{\alpha\alpha}}{f_{MHD}}$ is between 0.025 and 0.125, which supports efficient heating of electrons by the magnetic pumping mechanism. The Lichko et al. (2017) study modeled the effects of magnetic pumping assuming a generic pitch angle diffusion mechanism and a range of pitch angle diffusion rates; here, we have calculated the diffusion rate ($D_{\alpha\alpha}$) explicitly based on the whistler observations. The probable obliqueness of these whistler waves means that a significant parallel electric field component likely also exists and may provide additional heating of electrons via Landau damping during magnetic compressions.

4.3. Effects of Magnetic Pumping on the Electron Distribution Function

Sections 4.1 and 4.2 demonstrated that efficient wave-particle interactions can occur during the magnetic compressions observed and that the observed whistlers can thus be expected to isotropize (to some degree) the electron distribution function. The observed phase shift of $\frac{\pi}{5}$ between the ratio of the perpendicular-to-parallel electron temperatures, and the compressive wave fronts (Figure 2, insert), suggests that pitch angle diffusion, and subsequent heating, does indeed occur, and we demonstrate the effect of this diffusion on the superthermal electron distribution function (DF) in Figure 4.

The left-hand column shows DF for f_{pe}/f_{ce}~50 (efficient diffusion) and the right column shows DF for f_{pe}/f_{ce}~120 (about an order of magnitude smaller diffusion rate). The top panels show DF transverse to the local magnetic field (red), while the middle row shows DF parallel to the local magnetic field (blue). Solid (dashed) lines indicate DF at times of magnetic field maxima (minima). The effects of magnetic pumping are similar at both values of f_{pe}/f_{ce} for electrons transverse to the local magnetic field (panels a and d). The effects for the parallel distribution function, however, indicate an importance of pitch angle diffusion efficiency: for lower f_{pe}/f_{ce}, significant parallel heating is observed (panel b), while at higher f_{pe}/f_{ce} the parallel distribution function does not change (panel e).

Panels (c) and (f) show the ratio of DF minus one, in each column, at the maximum-to-minimum in magnetic field strengths (i.e., solid lines divided by the dashed lines, minus one, for each color). The resultant heating observed for the lower value of f_{pe}/f_{ce} for electrons parallel to the magnetic field (blue line, panel c) occurs for all electron velocities, and is not observed in panel (f). This is consistent with the results of Lichko et al. (2017), who showed that heating through the magnetic pumping mechanism does not involve a specific resonant velocity (unlike Landau damping).

5. Discussion

The analysis presented in this case study demonstrates that magnetosonic waves are, under the right plasma conditions, able to heat ionospheric superthermal electrons at Mars through a combination of whistler wave generation and efficient pitch angle diffusion. The large-scale magnetosonic waves (or compressional magnetic pumping) modulate the superthermal electron pitch angle distribution via the conservation of the first magnetic adiabatic moment, driving temperature anisotropies which lead to the generation of whistler waves during the compressive wave fronts (Figure 2). Subsequent wave-particle interactions mean that these whistler waves act back on the superthermal electron distribution function to isotropize the plasma, in an attempt to drive T_{perp} back equal to T_{para}. The local plasma conditions suggest that efficient wave-particle interactions and pitch angle diffusion occur, and analysis of the superthermal electron distribution function confirms this (Figure 4). This efficient pitch angle diffusion breaks the adiabaticity of the large-scale magnetosonic waves, leading to heating of the superthermal electrons during magnetic decompression. Evidence of this heating is observed as the phase shift between the ratio of the perpendicular-to-parallel electron temperatures, and the magnetosonic wave fronts (Figure 2). The observations presented here agree with model results by Lichko et al. (2017).

For the case study analyzed here, superthermal electron temperatures were raised from a background value of ~5 eV up to 7–8 eV (Figure 3a). The superthermal electrons gain some of the compression energy due to isotropization of the distribution via pitch angle scattering. An estimate of the maximum heating rate with the assumption that the superthermal electron distribution is fully isotropized by whistlers during compression, gives 10^{-3} eV/s per electron. Such a heating rate would require that superthermal electrons be exposed to the magnetosonic waves for ~1,000 s (equivalent to ~40 compression cycles) in order to gain 1 eV in energy. It is not clear how realistic such a timescale is, but Lichko et al. (2017) note that multiple compression cycles are necessary to significantly heat plasma through this mechanism, and our heating rate appears to be consistent with their results. We emphasize that this is a ball park estimate of the superthermal electron heating rate, and a self consistent study that includes all relevant physics is required to conclusively determine this.

The superthermal electron population is an important energy source for ionospheric thermal electrons in planetary ionospheres. The ionospheric thermal electron temperature is an important parameter because it can significantly influence the rates of chemical reactions and subsequent ionospheric structure (Schunk & Nagy, 2009). The thermal electron temperature is influenced by a number of energy sources and sinks in the Martian ionosphere: superthermal electrons produced from photoionization of atmospheric neutrals, and from the solar wind and magnetosheath, can heat the thermal electron population via collisions (e.g., Fox & Dalgarno, 1979; Fox, 1988; Matta et al., 2014; Sakai et al., 2015, 2016; Torr et al., 1980). Collisional cooling between thermal electrons and ions and atmospheric neutrals, along with conductive heat transport, act to reduce the thermal electron temperature. Studies of the Martian ionospheric energy budget have shown that the thermal electron temperature is significantly warmer than model predictions above altitudes of ~250 km, and topside heat fluxes, driven by the Mars-solar wind interaction, have been suggested as possible sources for this additional energy (Chen et al., 1978; Choi et al., 1998; Cui et al., 2015; Hanson & Mantas, 1988).

The unmagnetized nature of Mars's magnetosphere means that the solar wind stand off distance from the Martian subsolar point can be comparable to typical plasma length scales there (e.g., the proton gyroradius), and it has long been expected that solar wind energy may be directly deposited to the upper ionosphere via wave-particle interactions induced by the solar wind interaction with the planetary obstacle (Cloutier et al., 1969; Cloutier & Daniell, 1979; Ergun et al., 2006; Moses et al., 1988). The heating of ionospheric superthermal electrons via magnetic pumping, as reported in this study, demonstrates one plausible energy deposition mechanism. Additional studies are needed to fully quantify the importance of this heating.

Whistler waves have also been observed at the boundary between the shocked solar wind plasma and the dayside upper ionosphere at Venus (Scarf et al., 1979; Strangeway & Russell, 1996). Observed wave power substantially decreased as the spacecraft traversed from the shocked solar wind into the upper ionosphere, and it has been suggested that these whistler waves are damped as they heat ionospheric electrons via Landau damping (Scarf et al., 1980; Taylor et al., 1979). More recent analysis has however questioned how efficient such damping would be at heating the ionosphere. Szegö et al. (1991) noted that the magnetic field is typically in a draped configuration at the top of the Venusian ionosphere, meaning that the magnetic field is to first-order horizontal relative to the upper ionospheric boundary, and whistler waves (which tend to carry energy parallel to the magnetic field) would be unable to penetrate far into the ionosphere. Such limitations also apply at Mars, however, the study presented here demonstrates that the large-scale magnetic compressions are able to generate whistler waves at ever greater depths in the ionosphere because the compressive wave fronts travel perpendicular to the draped magnetic field. Such a mechanism could explain the Venus observations and to our knowledge, has not been proposed before. Although few studies exist, magnetosonic waves have been observed at the Venusian bow shock (Shan et al., 2014), and more work is needed to investigate the feasibility of this mechanism.

6. Conclusions

The unmagnetized nature of the Martian magnetosphere leads to a complex interaction between the planetary ionosphere and the solar wind. We have presented observations of large-scale magnetosonic waves (likely produced by the Mars-solar wind interaction) propagating into the Martian upper ionosphere. An earlier study of the event presented here demonstrated that such large-scale waves were able to directly heat the heavy, cold ionospheric ions (Fowler et al., 2018). This study demonstrates that these magnetosonic waves are also able to heat ionospheric superthermal electrons via the magnetic pumping mechanism described by, for example, Lichko et al. (2017) and Borovsky et al. (2017). The large-scale compressive wave fronts modulate the superthermal electron pitch angle distribution via conservation of the first magnetic adiabatic invariant, leading to the generation of whistler waves. When plasma conditions allow for efficient wave-particle interactions (as is the case in this study), the induced whistlers act back on the superthermal electron population, and pitch angle diffusion acts to reduce the temperature anisotropy between T_{perp} and T_{para}. This pitch angle diffusion breaks the adiabaticity of the large- scale magnetosonic wave and leads to heating of the superthermal electrons during magnetic decompression. The observed phase shift between the ratio of perpendicular-to-parallel superthermal electron temperatures, and the compressive wave fronts, also supports this heating mechanism. In the presented case study the superthermal electron temperature was enhanced from ~5 eV up to 7–8 eV when plasma conditions were supportive of efficient pitch angle diffusion.

The observed coupling between the solar wind and Mars's upper ionosphere provides a topside ionospheric energy influx, which has long been predicted to be an important factor in explaining observed enhanced electron temperatures in the Martian (and Venusian) upper ionospheres. Future work is needed to fully quantify the importance of this magnetic pumping and heating mechanism at both bodies.

Acknowledgments
Work at SSL and LASP was supported by NASA funding for the MAVEN project through the Mars Exploration Program under Grant NNH10CC04C. The work of O. V. Agapitov was supported by NASA Grant 80NSSC19K0848 and NSF Grant 1914670. Data used in this study are available on the NASA Planetary Data System (https://pds.nasa.gov/).

References

Adam, J. (1987). Review of tokamak plasma heating by wave damping in the ion cyclotron range of frequency. *Plasma Physics and Controlled Fusion*, *29*(4), 443.

Agapitov, O., Artemyev, A. V., Mourenas, D., Mozer, F., & Krasnoselskikh, V. (2015). Nonlinear local parallel acceleration of electrons through Landau trapping by oblique whistler mode waves in the outer radiation belt. *Geophysical Research Letters*, *42*, 10,140–10,149. https://doi.org/10.1002/2015GL066887

Agapitov, O., Drake, J. F., Vasko, I., Mozer, F. S., Artemyev, A., Krasnoselskikh, V., et al. (2018). Nonlinear electrostatic steepening of whistler waves: The guiding factors and dynamics in inhomogeneous systems. *Geophysical Research Letters*, *45*, 2168–2176. https://doi.org/10.1002/2017GL076957

Agapitov, O., Mourenas, D., Artemyev, A., Hospodarsky, G., & Bonnell, J. (2019). Time scales for electron quasi-linear diffusion by lower-band chorus waves: The effects of $\omega pe/\Omega ce$ dependence on geomagnetic activity. *Geophysical Research Letters*, *46*, 6178–6187. https://doi.org/10.1029/2019GL083446

Agapitov, O. V., Mourenas, D., Artemyev, A. V., & Mozer, F. S. (2016). Exclusion principle for very oblique and parallel lower band chorus waves. *Geophysical Research Letters*, *43*, 11,112–11,120. https://doi.org/10.1002/2016GL071250

Andersson, L., Ergun, R., Delory, G., Eriksson, A., Westfall, J., Reed, H., et al. (2015). The Langmuir probe and waves (LPW) instrument for MAVEN. *Space Science Reviews*, *195*(1-4), 173–198.

André, M., & Yau, A. (1997). Theories and observations of ion energization and outflow in the high latitude magnetosphere. *Space Science Reviews*, *80*(1-2), 27–48.

Artemyev, A., Agapitov, O., Mourenas, D., Krasnoselskikh, V., & Mozer, F. (2015). Wave energy budget analysis in the Earth's radiation belts uncovers a missing energy. *Nature Communications*, *6*, 7143.

Artemyev, A., Agapitov, O., Mourenas, D., Krasnoselskikh, V., Shastun, V., & Mozer, F. (2016). Oblique whistler-mode waves in the Earth's inner magnetosphere: Energy distribution, origins, and role in radiation belt dynamics. *Space Science Reviews*, *200*(1-4), 261–355.

Artemyev, A. V., Mourenas, D., Agapitov, O. V., & Krasnoselskikh, V. V. (2013). Parametric validations of analytical lifetime estimates for radiation belt electron diffusion by whistler waves. *Annales Geophysicae*, *31*(4), 599–624. https://doi.org/10.5194/angeo-31-599-2013

Barker, A., Li, X., & Selesnick, R. (2005). Modeling the radiation belt electrons with radial diffusion driven by the solar wind. *Space Weather*, *3*, S10003. https://doi.org/10.1029/2004SW000118

Borovsky, J. E., & Hansen, P. J. (1990). The magnetic pumping of plasmas with sawtooth waveforms. *Physics of Fluids B: Plasma Physics*, *2*(6), 1114–1127.

Borovsky, J. E., Horne, R. B., & Meredith, N. P. (2017). The contribution of compressional magnetic pumping to the energization of the Earth's outer electron radiation belt during high-speed stream-driven storms. *Journal of Geophysical Research: Space Physics*, *122*, 12,072–12,089. https://doi.org/10.1002/2017JA024607

Brautigam, D., & Albert, J. (2000). Radial diffusion analysis of outer radiation belt electrons during the October 9, 1990, magnetic storm. *Journal of Geophysical Research*, *105*(A1), 291–309.

Chen, R., Cravens, T., & Nagy, A. (1978). The Martian ionosphere in light of the Viking observations. *Journal of Geophysical Research*, *83*(A8), 3871–3876.

Choi, Y., Kim, J., Min, K., Nagy, A., & Oyama, K. (1998). Effect of the magnetic field on the energetics of Mars ionosphere. *Geophysical Research Letters*, *25*(14), 2753–2756.

Cloutier, P., & Daniell, R. Jr. (1979). An electrodynamic model of the solar wind interaction with the ionospheres of Mars and Venus. *Planetary and Space Science*, *27*(8), 1111–1121.

Cloutier, P., McElroy, M., & Michel, F. (1969). Modification of the Martian ionosphere by the solar wind. *Journal of Geophysical Research*, *74*(26), 6215–6228.

Connerney, J. E. P., Espley, J., Lawton, P., Murphy, S., Odom, J., Oliversen, R., & Sheppard, D. (2015). The MAVEN magnetic field investigation. *Space Science Reviews*, *195*, 257–291. https://doi.org/10.1007/s11214-015-0169-4

Cui, J., Galand, M., Zhang, S., Vigren, E., & Zou, H. (2015). The electron thermal structure in the dayside Martian ionosphere implied by the MGS radio occultation data. *Journal of Geophysical Research: Planets*, *120*, 278–286. https://doi.org/10.1002/2014JE004726

Drake, J. F., Agapitov, O. V., & Mozer, F. S. (2015). The development of a bursty precipitation front with intense localized parallel electric fields driven by whistler waves. *Geophysical Research Letters*, *42*, 2563–2570. https://doi.org/10.1002/2015GL063528

Ergun, R., Andersson, L., Peterson, W., Brain, D., Delory, G., Mitchell, D., et al. (2006). Role of plasma waves in Mars' atmospheric loss. *Geophysical Research Letters*, *33*, L14103. https://doi.org/10.1029/2006GL025785

Ergun, R. E., Morooka, M. W., Andersson, L. A., Fowler, C. M., Delory, G. T., Andrews, D. J., et al. (2015). Dayside electron temperature and density profiles at Mars: First results from the MAVEN Langmuir probe and waves instrument. *Geophysical Research Letters*, *42*, 8846–8853. https://doi.org/10.1002/2015GL065280

Fowler, C., Andersson, L., Ergun, R., Harada, Y., Hara, T., Collinson, G., et al. (2018). MAVEN observations of solar wind-driven magnetosonic waves heating the Martian dayside ionosphere. *Journal of Geophysical Research: Space Physics*, *123*, 4129–4149. https://doi.org/10.1029/2018JA025208

Fowler, C. M., Andersson, L., Halekas, J., Espley, J. R., Mazelle, C., Coughlin, E. R., et al. (2017). Electric and magnetic variations in the near-Mars environment. *Journal of Geophysical Research: Space Physics*, *122*, 8536–8559. https://doi.org/10.1002/2016JA023411

Fox, J. L. (1988). Heating efficiencies in the thermosphere of Venus reconsidered. *Planetary and space science*, *36*(1), 37–46.

Fox, J. L., & Dalgarno, A. (1979). Ionization, luminosity, and heating of the upper atmosphere of Mars. *Journal of Geophysical Research*, *84*(A12), 7315–7333.

Gary, S. P., & Wang, J. (1996). Whistler instability: Electron anisotropy upper bound. *Journal of Geophysical Research*, *101*(A5), 10,749–10,754.

Hanson, W., & Mantas, G. (1988). Viking electron temperature measurements: Evidence for a magnetic field in the Martian ionosphere. *Journal of Geophysical Research*, *93*(A7), 7538–7544.

Horne, R., Glauert, S., & Thorne, R. (2003). Resonant diffusion of radiation belt electrons by whistler-mode chorus. *Geophysical Research Letters*, *30*(9), 1493. https://doi.org/10.1029/2003GL016963

Horne, R. B., Thorne, R. M., Glauert, S. A., Albert, J. M., Meredith, N. P., & Anderson, R. R. (2005). Timescale for radiation belt electron acceleration by whistler mode chorus waves. *Journal of Geophysical Research*, *110*, A03225. https://doi.org/10.1029/2004JA010811

Jakosky, B. M., Lin, R., Grebowsky, J., Luhmann, J., Mitchell, D., Beutelschies, G., et al. (2015). The Mars atmosphere and volatile evolution (MAVEN) mission. *Space Science Reviews*, *195*(1-4), 3–48.

Kennel, C. F., & Petschek, H. (1966). Limit on stably trapped particle fluxes. *Journal of Geophysical Research*, *71*(1), 1–28.

Laroussi, M., & Roth, J. R. (1989). Theory of first-order plasma heating by collisional magnetic pumping. *Physics of Fluids B: Plasma Physics*, *1*(5), 1034–1041.

Li, W., Mourenas, D., Artemyev, A., Agapitov, O., Bortnik, J., Albert, J., et al. (2014). Evidence of stronger pitch angle scattering loss caused by oblique whistler-mode waves as compared with quasi-parallel waves. *Geophysical Research Letters*, *41*, 6063–6070. https://doi.org/10.1002/2014GL061260

Lichko, E., Egedal, J., Daughton, W., & Kasper, J. (2017). Magnetic pumping as a source of particle heating and power-law distributions in the solar wind. *Astrophysical Journal Letters*, *850*(2), L28.

Lundin, R., Winningham, D., Barabash, S., Frahm, R., Andersson, H., Holmström, M., et al. (2006). Ionospheric plasma acceleration at Mars: ASPERA-3 results. *Icarus*, *182*(2), 308–319.

Lyons, L. R., Thorne, R. M., & Kennel, C. F. (1972). Pitch-angle diffusion of radiation belt electrons within the plasmasphere. *Journal of Geophysical Research*, *77*(19), 3455–3474.

Matta, M., Galand, M., Moore, L., Mendillo, M., & Withers, P. (2014). Numerical simulations of ion and electron temperatures in the ionosphere of Mars: Multiple ions and diurnal variations. *Icarus*, *227*, 78–88.

McFadden, J., Kortmann, O., Curtis, D., Dalton, G., Johnson, G., Abiad, R., et al. (2015). MAVEN Suprathermal and thermal ion compostion (STATIC) instrument. *Space Science Reviews*, *195*(1-4), 199–256.

Mitchell, D., Mazelle, C., Sauvaud, J.-A., Thocaven, J.-J., Rouzaud, J., Fedorov, A., et al. (2016). The MAVEN solar wind electron analyzer. *Space Science Reviews*, *200*(1-4), 495–528.

Miyoshi, Y., Jordanova, V., Morioka, A., Thomsen, M., Reeves, G., Evans, D., & Green, J. (2006). Observations and modeling of energetic electron dynamics during the October 2001 storm. *Journal of Geophysical Research*, *111*, A11S02. https://doi.org/10.1029/2005JA011351

Miyoshi, Y., Morioka, A., Misawa, H., Obara, T., Nagai, T., & Kasahara, Y. (2003). Rebuilding process of the outer radiation belt during the 3 November 1993 magnetic storm: NOAA and Exos-D observations. *Journal of Geophysical Research*, *108*(A1), 1004. https://doi.org/10.1029/2001JA007542

Morschhauser, A., Lesur, V., & Grott, M. (2014). A spherical harmonic model of the lithospheric magnetic field of Mars. *Journal of Geophysical Research: Planets*, *119*, 1162–1188. https://doi.org/10.1002/2013JE004555

Moses, S., Coroniti, F., & Scarf, F. (1988). Expectations for the microphysics of the Mars-solar wind interaction. *Geophysical Research Letters*, *15*(5), 429–432.

Mourenas, D., Artemyev, A., Agapitov, O., Krasnoselskikh, V., & Mozer, F. (2015). Very oblique whistler generation by low-energy electron streams. *Journal of Geophysical Research: Space Physics*, *120*, 3665–3683. https://doi.org/10.1002/2015JA021135

Porkolab, M., Lloyd, B., Takase, Y., Bonoli, P., Fiore, C., Gandy, R., et al. (1984). High-power electron Landau-heating experiments in the lower hybrid frequency range in a tokamak plasma. *Physical Review Letters*, *53*(13), 1229.

Sakai, S., Andersson, L., Cravens, T. E., Mitchell, D. L., Mazelle, C., Rahmati, A., et al. (2016). Electron energetics in the Martian dayside ionosphere: Model comparisons with MAVEN data. *Journal of Geophysical Research: Space Physics*, *121*, 7049–7066. https://doi.org/10.1002/2016JA022782

Sakai, S., Rahmati, A., Mitchell, D. L., Cravens, T. E., Bougher, S. W., Mazelle, C., et al. (2015). Model insights into energetic photoelectrons measured at Mars by MAVEN. *Geophysical Research Letters*, *42*, 8894–8900. https://doi.org/10.1002/2015GL065169

Scarf, F., Taylor, W., & Green, I. (1979). Plasma waves near Venus: Initial observations. *Science*, *203*(4382), 748–750.

Scarf, F., Taylor, W., Russell, C., & Elphic, R. (1980). Pioneer Venus plasma wave observations: The solar wind-Venus interaction. *Journal of Geophysical Research*, *85*(A13), 7599–7612.

Schunk, R., & Nagy, A. (2009). *Ionospheres: Physics, plasma physics, and chemistry*. Cambridge: Cambridge University Press.

Seo, S.-H., Chung, C., & Chang, H.-Y. (2000). Review of heating mechanism in inductively coupled plasma. *Surface and Coatings Technology*, *131*(1-3), 1–11.

Shan, L., Lu, Q., Wu, M., Gao, X., Huang, C., Zhang, T., & Wang, S. (2014). Transmission of large-amplitude ULF waves through a quasi-parallel shock at Venus. *Journal of Geophysical Research: Space Physics*, *119*, 237–245. https://doi.org/10.1002/2013JA019396

Strangeway, R. J., & Russell, C. T. (1996). Plasma waves and field-aligned currents in the Venus plasma mantle. *Journal of Geophysical Research*, *101*(A8), 17,313–17,324.

Summers, D., Thorne, R. M., & Xiao, F. (1998). Relativistic theory of wave-particle resonant diffusion with application to electron acceleration in the magnetosphere. *Journal of Geophysical Research*, *103*(A9), 20,487–20,500.

Szegö, K., Shapiro, V., Shevchenko, V., Sagdeev, R., Kasprzak, W., & Nagy, A. (1991). Physical processes in the plasma mantle of Venus. *Geophysical Research Letters*, *18*(12), 2305–2308.

Taylor, W., Scarf, F., Russell, C., & Brace, L. (1979). Absorption of whistler mode waves in the ionosphere of Venus. *Science*, *205*(4401), 112–114.

Torr, M. R., Richards, P., & Torr, D. (1980). A new determination of the ultraviolet heating efficiency of the thermosphere. *Journal of Geophysical Research*, *85*(A12), 6819–6826.